GEOPHYSICS, VOL. 67, NO. 5 (SEPTEMBER-OCTOBER 2002); P. 1364–1371, 8 FIGS., 1 TABLE.
10.1190/1.1512741

Case History

3-D tomographic seismic inversion of a paleochannel system in central New South Wales, Australia

Tara Deen* and Karsten Gohl‡

ABSTRACT

Buried paleochannels are of significant interest for understanding hydrological mechanisms and their potential as alluvial gold deposits. Seismic tomographic methods are a suitable solution for resolving the vertical and horizontal structure of such features. We assess a method for seismic 3-D tomographic inversion from refraction arrivals with reflection control over a suspected paleochannel adjacent to the Wyalong gold fields in the Lachlan fold belt of central New South Wales, Australia. A standard multichannel engineering seismic recording and cable–receiver system was used on a 3-D field geometry of multiple linear arrays. More than 3000 P-wave first-arrival traveltime values were inverted using a regularized inversion scheme for which simplified 2-D models served as initial velocity–depth models for the complete 3-D inversion. Seismic reflection arrivals provided additional depth estimates to the bedrock and compensated for a lack of refraction phases at that depth. Correlating the 3-D seismic velocity–depth data with existing drillhole and nonseismic geophysical data resulted in a detailed structural and compositional interpretation of the paleochannel and the incised regolith. The model suggests the presence of a system of deposits from meandering channels overlying a metasedimentary bedrock formation. The general paleodrainage deposit is relatively conductive in electromagnetic surveys, indicating a potential saline storage or transport mechanism.

INTRODUCTION

Modeling 2-D in-line seismic refraction data is standard practice in geotechnical and groundwater exploration applications, but the analysis and inversion of 3-D seismic refraction/reflection data in these applications is less common. Tomography is a common tool for crosshole seismic recordings, but rarely is it used in a surface seismic survey for groundwater or geotechnical applications. Examples of 3-D velocity imaging in the shallow subsurface may be seen in Lanz et al. (1998) and Brzostowski and McMechan (1992). As part of the multiinstitutional Australian Gilmore project, our experiment tested the efficiency of a surface refraction tomography field geometry for delineating a complex shallow subsurface structure. The Gilmore project was a comprehensive program of acquiring geophysical data over buried paleochannels (part of the paleo-Lachlan River system) adjacent to the Wyalong gold field in the Lachlan fold belt (Lawrie, 1999).

The target survey was a suspected buried paleochannel in the Lachlan fold belt region, near West Wyalong in central New South Wales, Australia (Figure 1). Little geophysical exploration, aside from regional-scale aerial data for geological mapping, had been undertaken in this area prior to 1998. As part of the Gilmore project, additional airborne and ground electromagnetic (EM), gamma-ray spectrometric, and airborne and ground magnetic data were acquired. High-resolution airborne magnetic mapping made the delineation of the paleochannel systems in this region possible because the deposits contain highly magnetic detrital ferruginous (maghemitic) pisoliths in lenses within sand and clay (Munday et al., 2000). The surface lithology of the region is characterized by a stagnant depositional alluvial environment (Gibson and Chan, 1999). Surface expression of bedrock in the region is subtle, with little outcrop evident. Most bedrock is covered by a Quaternary regolith, primarily sourced from paleodrainage deposits. Cuttings in the region (Mackey et al., 2000) and regolith drill data indicate the

Manuscript received by the Editor January 23, 2001; revised manuscript received March 18, 2002.
*Formerly Macquarie University, Department of Earth & Planetary Sciences and CRC AMET, Sydney, New South Wales 2109, Australia; currently University of Sydney, School of Geosciences, Sydney, New South Wales 2006, Australia. E-mail: tara@es.usyd.edu.au.
‡Formerly Macquarie University, Department of Earth & Planetary Sciences and CRC AMET, Sydney, New South Wales 2109, Australia; currently Alfred Wegener Institute for Polar and Marine Research, Postfach 120161, D-27515 Bremerhaven, Germany. E-mail: kgohl@awi-bremerhaven.de.

magnetic minerals within some paleochannel deposits may occur in discrete lenses of detrital magnetic ferruginous pisoliths, deposited in paleochannels incised into the regolith at approximately 10 m depth. Adjacent to the field site, the Yiddah Formation, a Silurian–Devonian sandstone, siltstone, and minor conglomerate formation, emerges as a low outcrop surrounded by a region of Quaternary colluvium and alluvium scree. We can expect that detrital materials of the channel fill provide sufficient acoustic impedance contrast to the incised regolith for discrimination in a seismic velocity field. A nearby rotary air blast (RAB) drill provided a lithological log for comparison; however, no seismic velocities were available for this area.

The study was conducted to identify the minimum amount of data required to effectively utilize seismic refraction tomography as a valid exploration tool. We demonstrate that seismic refraction tomography is a viable tool in delineating such a buried paleochannel system, but we also show its limitations.

SEISMIC DATA ACQUISITION AND PROCESSING

The seismic field geometry over a presumed branch of a paleochannel system consisted of eight linear arrays of 48 vertical-component 14-Hz geophones each (Figure 2). Each array recorded wavefields from up to 16 seismic shotpoints both in-line and off-line, covering an area of 400×400 m. Geophones were spaced 5 m apart on most receiver arrays, except for diagonal lines 7 and 8, which had 7-m spacing to allow for even geophone spacing and to fit the chosen geometry. We included diagonal lines to compensate for the lack of geophone arrays between existing lines and to create a quasi-circular geometry to avoid bias of preferred orientation, as well as to maximize the number of possible raypaths and reflection depth points for increased resolution. The surface expression of raypaths was calculated for each linear array of geophones (Figure 2), which then let us estimate the minimum number of shots required for the maximum ray coverage. This also enabled a variety of the azimuthal distribution of offsets and resulted in a maximum offset of 285 m on most lines in the survey and a maximum offset of 400 m on the diagonal lines. The approach resulted in recording 5088 seismic traces, of which 3046 traces were suitable for picking clearly identifiable first arrivals. Those traces not picked lacked the clarity for accurate first-arrival picking.

To take advantage of a mobile and repeatable seismic source, we used the IVI Mini-Vibrator of the Australian National Seismic Imaging Resource (ANSIR) as one of the two seismic sources. The vibrator was set for five sweeps at each vibrator point with an 8-s upsweep from 10 to 200 Hz. All seismic data were recorded with a Geometrics Strataview R48 seismograph at 1-ms intervals. The records were stacked prior to crosscorrelation with the vibrator sweep reference signal. We found that nonlinear near-source vibrator operating noise superposed first arrivals at short offsets. Therefore, we used a sledgehammer as the seismic source at selected shotpoints to derive thickness and velocities of the uppermost weathering layers. The field survey lasted 1.5 work days.

The seismic data were filtered with a band-pass filter of 50 to 200 Hz. Trace balancing and automatic gain control (AGC) did not improve the S/N ratio and consequently were not applied for first-arrival picking. First arrivals as well as reflection hyperbolae could be identified clearly throughout most recordings.

TOMOGRAPHIC MODELING

Traveltimes for the first P-wave arrivals were picked manually. The picked traveltimes of first P-wave arrivals of in-line recordings formed preliminary 2-D velocity–depth models—initial models for the 3-D inversion. A four-layer model of sediments underlain by bedrock is sufficient to fit most first-arrival branches in two dimensions. Our four-layer model was interpreted using ray tracing to forward model the manual picks (Figure 3). It consisted of a 2-m-thick surface layer

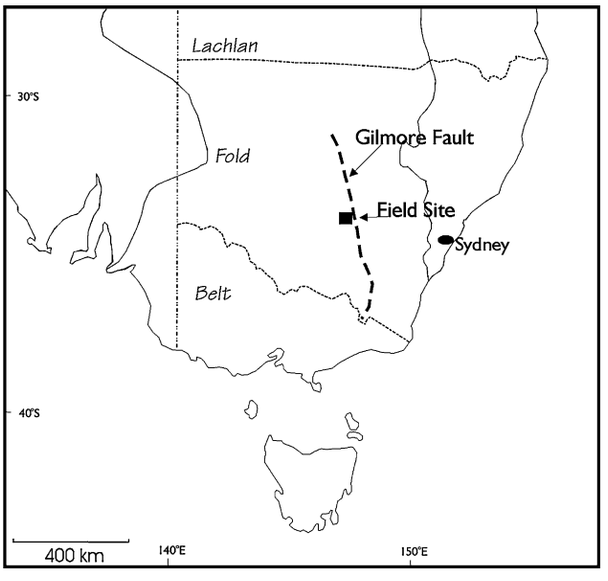

FIG. 1. Map of southeast Australia, showing the locations of the Lachlan fold belt, Gilmore fault, and survey field site.

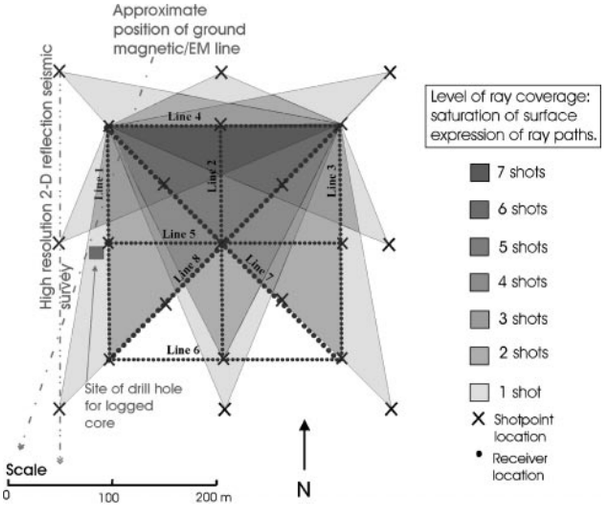

FIG. 2. Acquisition geometry for the field survey, showing the linear acquisition arrays, the 21 shotpoints, existing drillholes, and complementary survey sites. The surface expressions of raypaths were used to determine seismic ray coverage over the area and the minimum number of shots required to obtain adequate resolution.

with a P-wave velocity of 400 m/s, interpreted through direct observation as unconsolidated alluvium; a 9-m-thick second layer with a P-wave velocity of 1000 m/s, consistent with wet soil; and a 24-m-thick third layer with a P-wave velocity of 1600 m/s, consistent with wet soil, fine gravel, or sand. The fourth layer had a variable thickness, ranging between 60 and 90 m, with a P-wave velocity of 2300 m/s, interpreted as dense clay. These layers were underlain by a basement with a P-wave velocity of 4500 m/s, consistent with metasediments of the Yiddah Formation.

We conducted 3-D traveltime modeling by using an iterative first-arrival tomographic inversion package, in which a regularized inversion routine is computed rapidly over a regular 3-D grid using finite-difference extrapolation (Zelt and Barton, 1998). This routine was originally developed for deep crustal seismic refraction tomography but can be utilized for shallow subsurface imaging by appropriately adjusting model parameters. Only refraction first arrivals were used for the tomography; however, reflection information was used for the comparative interpretation.

Since a linearized inversion requires initial models, we interpolated between a pair of 2-D velocity–depth models in both the east–west and north–south directions. From this initial 3-D velocity–depth model, a series of iterations improved the model with respect to the picked traveltimes. Each subsequent iteration of the model was developed using both a finite-difference forward calculation of traveltimes and raypaths (Vidale, 1988, 1990) and a regularized inversion incorporating a combination of smallest, flattest, and smoothest perturbation constraints, the weights of each being allowed to vary with depth (Zelt and Barton, 1998). Velocity was not held as a constant. We found a node spacing of 5 m on a uniform grid appropriate with respect to the in-line geophone spacing. The inversion involved calculations on all 3046 picked first-arrival traveltimes from both in-line and off-line shotpoints. Inversions were iterated within a selected number of the calculated trade-off parameter λ, which is required to provide the model with a minimum structure for a given data misfit (Zelt and Barton, 1998). We ran the inversion over four iterations for each of four values of λ, resulting in 16 iterations. Each inversion sequence took a few minutes to complete on a medium- to high-end Unix workstation.

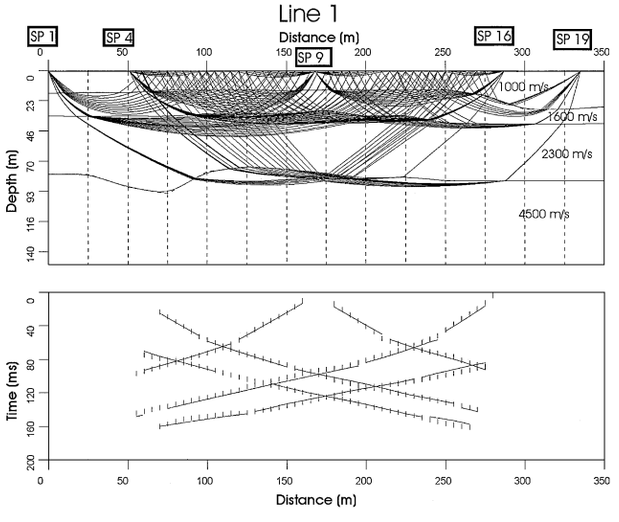

FIG. 3. Preliminary 2-D model corresponding to line 1. (top) Traced rays and the predicted model with depth. (bottom) Error bars for the picked traveltimes (vertical bars). The lines in the lower image are the predicted traveltimes for the model. Note that the layers are subhorizontal, with the bottom layer having a more variable depth to surface.

Although the traveltime fits of the 2-D in-line velocity–depth models gained a statistical χ^2 value close to one and rms traveltime residuals on the order of 2 to 3 ms, this accuracy was not achieved in the 3-D tomographic modeling process. Statistical values for the initial 3-D model were as high as a χ^2 of 20 with rms traveltime residuals of 10 000 ms. Four full inversion iterations reduced χ^2 to 17 for the inverted finite-difference processes and the ray tracing as low as 1.3 (forward modeling); rms traveltime residuals were reduced to 3000 ms at the final iteration. These traveltime residuals are still unreasonably high, and further iterations of the inversion process did not improve them. However, the χ^2 values for the forward modeling show promise. We may have been too efficient in decimating our data set at the acquisition stage, reducing ray penetration in many areas to a suboptimal point, which resulted in insufficient velocity control to adequately refine the model. Consequently, the accuracy of the model is highest in those areas with better resolution. We achieved better resolution in areas with greater ray penetration, such in the center of the cube and at depths where raypaths overlapped. Acceptable resolution was achieved in the midlayers, but only limited resolution was possible in the uppermost layer because of the limited-offset ray coverage available at shallow depths, a feature of the acquisition geometry. In addition, the limited offset meant that the refraction technique was adequately imaged the basement rock over the whole area. The identification of seismic reflection arrivals (see below) compensated for this problem.

The uppermost layer imaged in the tomographic cube is quite thin and not easily resolved using vibrator records. Most information about layer 1 comes from hammer shot records. The layer varies between 0.5 and 2 m, with an average thickness of 1 m, and has a seismic velocity of 400 m/s. Layer 2 has a seismic velocity of 1000 m/s, a mean thickness of 9 m, and moderate compositional homogeneity. However, because the shallowness of the layer means it is poorly controlled, the homogeneity may be a feature of limited resolution at that point in the tomographic cube. Layer 3 varies between 20 and 25 m thick and has an average seismic velocity of 1600 m/s. It shows a high heterogeneity, indicating a complex structure. Layer 4 has the most variable thickness—between 40 and 130 m—and has an average seismic velocity of 2300 m/s. It exhibits moderate to high compositional heterogeneity, most notably with increasing depth and proximity to the bedrock. Layer 5 has a seismic velocity of 4500 m/s. The depth to the surface of the layer is variable, ranging from 98 to 169 m over the survey area. Resolution of the fifth layer was poor in the refraction data because of the limited offsets used.

Horizontal depth slices from the top 30 m of the tomography cube (Figure 4) show residual influence from acquisition geometry as a result of the limited-offset ray coverage available at shallow depths. Between 40 and 70 m, a curved zone of lower relative velocity (1800–2200 versus 2600–3000 m/s) with a northeast–southwest trend is visible. This feature is evident in the four depth slices from 40 to 70 m, and its orientation

changes slightly with depth. Illustrated in Figure 5, this feature is interpreted as the paleochannel scour incised into layer 4 and infilled by layer 3. The velocity differences involved are subtle, but the curved outline of the feature indicates it is not an artifact from acquisition geometry but is a true velocity anomaly produced by the subsurface geology. Moreover, it correlates with the predominant strike of the large paleodrainage feature interpreted from aerial magnetic surveys (Mackey et al., 2000). The orientation and depth of this anomaly correlate with the conductive body imaged with ground EM data (Bartlett, 1999). The boundary between layers 3 and 4 in the vertical slices (Figure 5), which was well defined in the initial velocity model, ceases to be a sharply contrasted boundary in the 3-D inversion model. This is because of the interpreted paleochannel feature. The subtlety of the boundary indicates a lithological similarity between the two layers. Drilling has shown that the lithology of these two layers is similar (Table 1) because layer 3 is composed of interlayered clays and fine-grained pisolitic gravel beds and layer 4 is composed of clays and C-horizon slurry. However, a gradually increasing velocity is observed with increasing depth within these two layers.

The basement rock is visible in the 90-m depth slice, intersecting it at the top of the saddle-shaped feature evident in Figure 7.

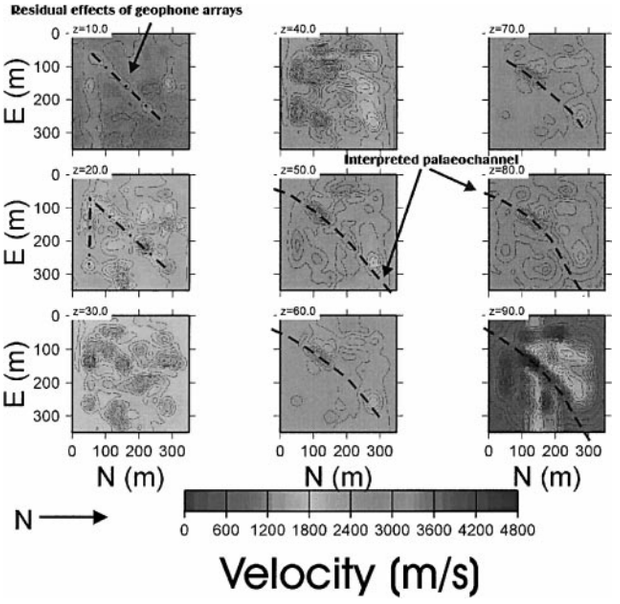

FIG. 4. Depth slices through a cube of the data after tomographic inversion. Depths (z) are in meters. Localizing seismic sampling directly around the geophone arrays is evident in the upper 30 m from limited offsets at shallow depths. A subtle curved feature, running roughly northeast–southwest, is visible between 40 and 70 m. This feature is coincident with a conductive feature seen between 30 and 80 m in the EM survey near the southwest corner of the tomographic cube and is interpreted as a paleochannel.

SEISMIC REFLECTIONS

Reflection hyperbolae (Figure 6) are visible in 22 individual seismic records, mostly in far-offset off-line recordings that we processed to map the reflector topography under the survey area. The strong amplitudes and first-depth estimates suggest this reflector coincides with the top of the metasedimentary Yiddah bedrock formation, identified from drillhole data outside our survey area. Imaging the bedrock using reflection points compensated for the limited refraction sampling of the bedrock and improved bedrock resolution. The identification of reflection arrivals was improved by trace balancing, a bandpass filter between 100 and 400 Hz, and AGC. The limited reflection data coverage did not permit any common midpoint (CMP) processing. However, we applied standard NMO corrections to derive the velocity for the surface-to-bedrock interval, independent of the traveltime inversion. An estimate of the NMO velocity accuracy resulted in a depth uncertainty of about 5 m. The resulting depth-to-bedrock values between 69 and 169 m were gridded and mapped across the survey area (Figure 7). The top-of-bedrock boundary exhibits a north-dipping trend at the western edge of the site and uneven features elsewhere over the survey area, forming a rough saddle shape with a northeast–southwest axis. The reflection information was used to constrain the location of the basement rock

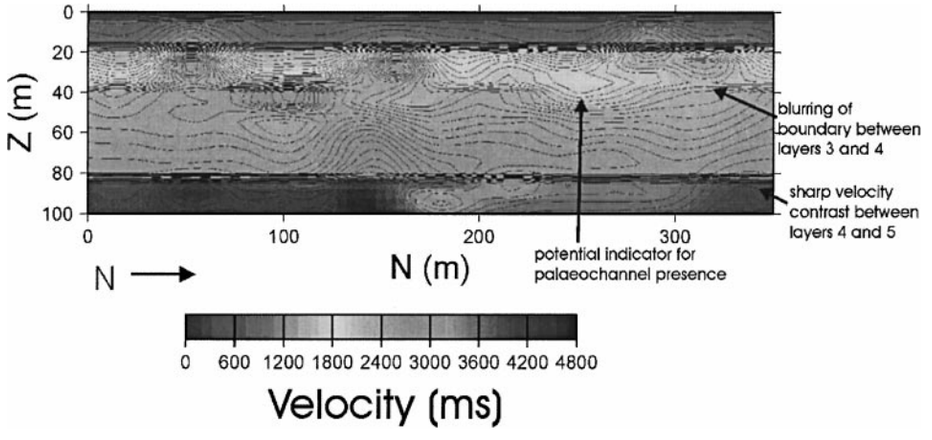

FIG. 5. A vertical north–south cross-section through the tomographic cube at 150 m east. The boundary blurs between the third and fourth layers, indicating a subtle transition between the two layers or a similarity in lithology. Lithologies of the layers can be seen in Table 1. The sharp velocity contrast between layers 4 and 5 is from the transition between the weathering layer and fresher rock at that point, the imposition of flat layers in the initial model, and a lack of refraction data control at that depth.

for the initial input model of the tomographic inversion. The reflection information also provided a useful constraint in the interpretation of the tomographic cube. There is good correlation between the features seen in the 90-m depth slice (Figure 4) and the basement rock profile (Figure 7). The saddle features seen on the bedrock are evident in the center of the depth slice section. Additionally, the profile of the reflection section indicates reduced resolution and thus reliability at the edges of the tomographic cue at that depth, noted by the continuation of bedrock velocities to the edges of the cube (suggesting a flat surface). The reflection data indicate the bedrock is in fact sloping downward toward the edges of the site.

Table 1. Interpretation of a logged company core taken adjacent to the survey area (Figure 2), with a comparison of the analogous interpreted seismic layers. Company data courtesy D. Gibson and R. Chan, Australian Geological Survey Organisation (AGSO).

Depth (m)			Equiv.
From	To	Description	Seismic Layer
0.0	0.5	Chocolate brown silty clays and sands	1
0.5	10	Clays and sandy gravels	2
10	21.5	Clays and pisolitic gravel beds	
21.5	31	Fine-grained pisolitic gravel beds	3
31	61	Milky gray clays (quartz rich from 51–57 m)	
61	72	Tan C-horizon slurry (very weathered saprolite)	4
72	93	Coarse-grained sandstone and micaceous siltstone	5

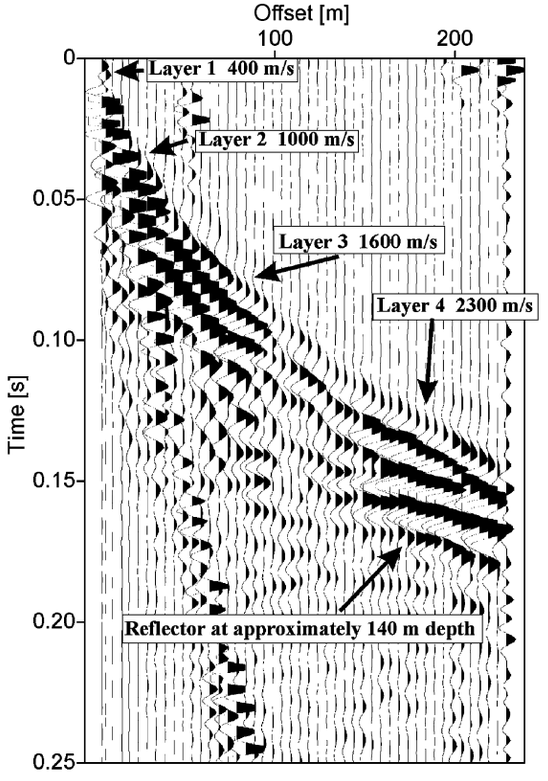

FIG. 6. Sample shot record typical of the area. This near-offset, in-line shot (taken adjacent to the end geophone of line 1) has a Vibroseis source. Four layers are distinct in the first P-wave arrivals. A reflector corresponding to the basement bedrock is also evident.

INTERPRETATION

Velocities and structures of the tomographic model (Figure 8) suggest a four-layer sedimentary system underlain by highly depth-variable bedrock. These interpreted layers correlate with the lithology of a logged RAB drill core obtained adjacent to the field site (Figure 2 and Table 1). Layer 1 (uppermost) varies between 0.5 and 2 m thick, with an average of 1 m, and has a P-wave velocity of 400 m/s. The interpretation of the lithology has been classified as a highly porous unconsolidated soil. This was derived from direct observation and drill core data.

Layer 2 has an average velocity of 1000 m/s and a mean thickness of 9 m. It exhibits moderate compositional homogeneity. The drill core suggests that the layer is composed of clays and sandy gravels. The velocity of the layer lies between the velocity of water and the low velocities for sand and clay. The layer is interpreted as a wet, interlayered clay and sandy gravel, and the interface between layers 1 and 2 is interpreted as the water table. Direct observation has shown that the water in this table is fresh, and RAB drill evidence suggests the water table may be perched (D. Gibson, 1999, personal communication) and potentially in hydrologic connection with a nearby dam.

Layer 3 varies in thickness between 20 and 25 m, with an average seismic velocity of 1600 m/s. The velocity field is highly heterogeneous, indicating a complex structure. This structure may indicate channel-fill sediments, which are highly variable

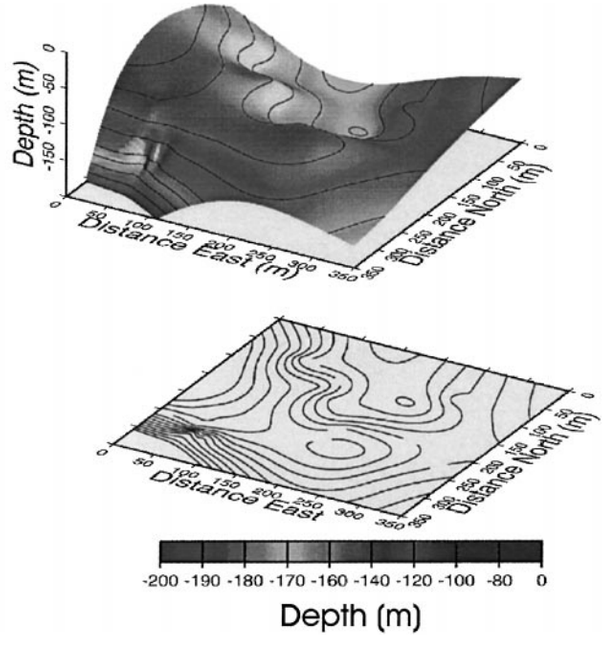

FIG. 7. Three-dimensional image illustrating the depth to the basement reflector over the tomographic survey area. (top) A 3-D representation of the contours. (bottom) Contours over the area. The view is from the northwest corner, looking to the southeast. Drillhole data and seismic velocities indicate the imaged surface is the fresh rock–saprolite interface.

both laterally and with depth. The velocity is consistent with a clay or gravel, potentially with water-filled pore spaces; this is confirmed by the drill cores, which consist of clays and pisolitic gravel beds. Preliminary studies suggest that a second water table lies at this depth (D. Gibson, 1999, personal communication).

Layer 4 has the most variable thickness and velocities, ranging between 40 and 130 m depth with average seismic velocities of 2200 m/s within the interpreted paleochannel sequence and 2600 m/s for the sediments around it. The paleochannel feature has been incised into this layer and infilled by the lower velocity layer 3 sediments. Drill cores from this depth interval (Table 1) show clays and C-horizon soil. The velocity field exhibits a moderate to high heterogeneity and can be interpreted to represent transitional stages between clays and bedrock-derived saprolite. At least some of the material in the layer has developed in-situ, as a result of weathering from the basement rock. This is indicated from the sediments in the drill data, which show that the lithology of the lower parts of this layer comprise very weathered saprolite, creating a C-horizon slurry formed from the bedrock. Seismic and drill core evidence indicate the transported in-situ boundary is most likely sited in the upper part of the fourth layer in the study area. The location of this boundary is important for identifying the source and history of regional regolith materials.

Layer 5 has an average seismic velocity of 4500 ± 200 m/s, consistent with the Silurian–Devonian Yiddah Formation—a lightly metamorphosed sandstone siltstone, and minor conglomerate that outcrops nearby. The depth to the surface of the layer is variable, with depths derived from reflection data ranging from 69 to 169 m and depths from the refraction data calculated as ranging from 86 to 169 m over the survey area. The layer exhibits a north-dipping trend at the western edge of the site and uneven features elsewhere, forming a rough saddle shape with a northeast–southwest axis. This irregularity may be the result of erosion when the formation was subaerial.

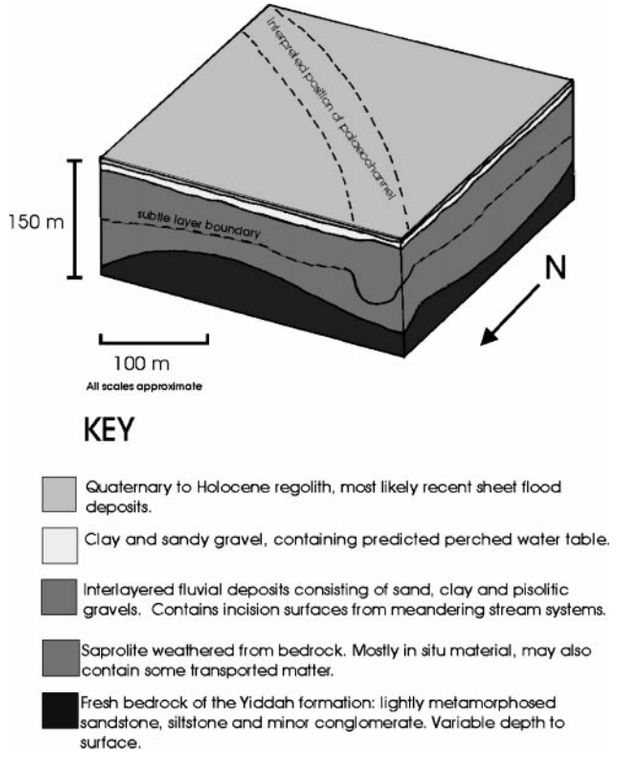

FIG. 8. Structural and compositional interpretation of the survey area, viewed from the northeast corner. A paleochannel visible in tomography and EM data is shown. Its predicted path is indicated in the surface of the block. The boundary between the fluvial deposits and saprolite is subtle and is sometimes not differentiable in seismic data.

All geological and geophysical techniques applied to the area as part of the Gilmore project led to a corresponding lithological model of the survey site. The presence of detrital ferruginous pisolith deposits with magnetic responses (Mackey et al., 2000) was confirmed by magnetic and airborne/ground EM surveys, along with drillhole data and recent landfill cuttings (Mackey et al., 2000) logged near the survey site. The pisoliths are located in lenses of gravel, which formed in paleochannel deposits in a northeast–southwest orientation at about 10 m depth in the seismic field area. The channel deposits were conductive in EM surveys in relation to the surrounding sediments and nearby paleochannel deposits. The relative conductivity of the paleochannels indicates they may be more saline than the surrounding rocks and regolith materials in the nearby Bland Creek paleovalley. This may indicate a mechanism for saline water transport or a series of salt-enriched silt and clay deposits. Knowledge of the distribution of paleochannel deposits in the region, both freshwater and saline, will assist in developing hydrogeological models for dryland salinity hazard assessment. Of the deposits, which Mackey et al. (2000) recognized in the Wyalong region, both saline and freshwater stores were identified. RAB drilling on the survey site (Gibson and Chan, 1999) identified a shallow, possibly perched freshwater aquifer with high variation in water levels. The surface of this water table was evident in the 3-D seismic refraction data by a clear velocity jump at approximately 18 m. A further aquifer potentially underlies this and may be more saline in nature.

As mentioned, the interpreted paleochannel feature incised into the fourth layer, evident in tomographic depth slices between depths of 40 and 70 m (Figure 4), was also imaged on ground magnetic and EM surveys (Bartlett, 1999). Drillhole data (Table 1) confirm that the lithology at this depth consists of clays and saprolite. While the maghemitic pisolith deposits are much shallower than this feature, drill data and aeromagnetic data indicate the ferruginous pisolith lenses follow roughly the same path as the channel imaged in the tomographic cube but at a depth of 10 to 15 m, just at the top of the predicted water table. This indicates the magnetically imaged, pisolith-filled lenses contained within relatively recent channels in the paleochannel system followed the same flow trends during deposition as the seismically imaged channel which formed earlier. Therefore, ground and surface water probably followed this path continuously for a large period of time. Unfortunately, there was insufficient resolution at 10 to 15 m depth to adequately control structure far off-line from the linear geophone arrays. Consequently, the pisolith lenses are too small to resolve with our survey design. A denser line spacing, while allowing for greater resolution at shallow depths, would have greatly increased the acquisition and processing costs of the survey.

A high-resolution north–south 2-D seismic reflection line was conducted along the western edge of the 3-D tomography survey site and continued southward from our survey site

(Leslie et al., 2000). This survey identified a north-dipping component of the Yiddah Formation, also visible on the western edge of the 3-D reflection imaging of the bedrock. The two methods imaged the bedrock at comparable depths. However, while the 2-D reflection data appear to indicate that the Yiddah Formation is dipping northward, the 3-D reflection data show that this is just a localized feature.

STRUCTURAL AND COMPOSITIONAL IMPLICATIONS

The survey site comprises a stagnant fluvial system which in turn overlies the bedrock of the Yiddah Formation. The upper layer of the section is a Quaternary or Holocene regolith, most likely recent sheetflood deposits. Sheetfloods are an occasional occurrence in the region. The water table is interpreted to be at the base of this layer, varying in depth from 1 to 2 m.

Below the surface soil lies a series of fluvial deposits of varying composition and thickness. The deposits are interpreted as interbedded sands, silts, clay, and gravel with concentrated lenses of pisolith beds. The interbedded sediments are interpreted to be a series of meandering gravel channels in a surrounding sea of alluvium (Lawrie et al., 1999; Deen et al., 2000). Those sediments, which host the pisolitic gravels, register a relatively strong magnetic susceptibility on aeromagnetic data. Some of the channels in this system have been imaged and identified in 3-D seismic tomography and airborne/ground EM data. While the results of the seismic tomographic inversion divide the fluvial deposits into three layers for modeling purposes, the sequence is most likely a more complex interlayered series of fluvial incisions and deposits.

This sedimentary deposit system is underlain by the bedrock of the Yiddah Formation. The surface of the formation is scoured and incised, indicating erosion events prior to the deposition of alluvium and burial of the bedrock and an unconformity at the interface. The erosional features have given the Yiddah Formation's fresh rock interface a saddle shape, with a general northward-dipping trend in the western side of the area and a deep scoured feature in the southwest quadrant (Figure 7). Streams probably eroded the Yiddah Formation prior to burial.

The interpreted lithology of the subsurface suggests that the paleoenvironment underwent both depositional and erosional episodes, with depositional alluvial and fluvial environments being the most common. The mixed-load meandering stream theory is given further weight by the composition of the sediments present in drillhole data (Table 1). Streams in a meandering system migrate laterally, but the main channel body remains more or less constant (Collinson, 1996).

The presence of alluvial gold in the Parkes, Forbes, and Temora gold fields (Downes and Burton, 1999) is a positive indicator of the potential for alluvial gold in some paleochannels in the region. However, the Yiddah paleodrainage deposits have been formed from a provenance, so it is unlikely they have sampled auriferous deposits (Lawrie, K., 1999, personal communication).

The indication of the presence of a saline water storage or transport mechanism within the paleochannel is an important factor in dryland salinity risk assessment for the area. Groundwater may follow the path of the maghaemitic pisolith-rich channel deposits because they have the highest gravel content and, consequently, the greatest potential porosity. However, the presence of a perched freshwater aquifer (<2 m depth) indicates that surface soil salinity is not a risk for the Yiddah site.

CONCLUSIONS

We deployed a multichannel seismic system in various linear array settings to record first arrivals and reflected phases to test the viability of a 3-D tomographic inversion for delineating a paleochannel system in central New South Wales, Australia. Constraints from nonseismic geophysical as well as drillhole data supported the model-building process. The interpreted tomographic velocity–depth model consists of a shallow surface alluvium layer overlying a series of interbedded sands, silts, clays, and gravel with some pisolith lenses. These sediments form the deposits of a mixed-load, meandering stream system underlain by a metasedimentary bedrock formation. The subsurface lithology suggests that the paleoenvironment underwent a series of both depositional and erosional episodes, with depositional alluvial/fluvial environments being the most common.

A relatively large and densely sampled data set, required for a successful 3-D tomographic inversion for near-surface targets such as paleochannels, can be acquired very efficiently using variable linear arrays with a standard engineering multichannel recording system. Improvements in the optimization of shot and receiver locations with respect to target depth and in the efficiency of the inversion process can further speed the process from acquisition to building a reliable model.

The location of the paleochannel and its water flow and water composition are essential for understanding dryland salinity in the area. Further knowledge of the lithology and sediment source for paleochannels in this area will increase the potential for discovering alluvial gold sources from nearby auriferous deposits, although the source rock for the channel surveyed for this study is not located near the mineralized sites.

ACKNOWLEDGMENTS

This work was completed with the aid of a Co-operative Research Centre for Australian Mineral Technologies (CRC AMET) scholarship to T. Deen and an ASEG Research Foundation Grant and a Macquarie University Research Grant to K. Gohl. The authors would like to thank AGSO, Australian National Seismic Imaging Resource (ANSIR), Co-operative Research Centre for Landscape Environments and Mineral Evolution (CRC LEME), and CRC AMET for technical assistance and for providing access to supplementary data sets. The fieldwork was completed as part of the Gilmore project in conjunction with AGSO, (CRC LEME), and CRC AMET and with the personal assistance of Eva Papp, Chris Leslie, Kevin Wake-Dyster, Heike Apps, and Alex Takken. Data were recorded with the Strataview seismograph of Macquarie University and the IVI Mini-Vibrator of ANSIR. Processing and modeling were accomplished with Seismic Un*x, GLOBE Claritas™, RAYINVR and FAST software packages (the latter two developed by C. Zelt) and were imaged with GMT (Generic Mapping Tools by Wessel and Smith). This is publication number 297 of the National Key Centre for Geochemical Evolution and Metallogeny of Continents (GEMOC).

REFERENCES

Bartlett, B., 1999, The use of geophysical techniques in delineating paleochannels near Wyalong, NSW: B.Sc. (Hons) thesis, CRC AMET, Curtin University.

Brzostowski, M. A., and McMechan, G. A., 1992, 3-D tomographic imaging of near-surface seismic velocity and attenuation: Geophysics, **57**, 396–403.

Collinson, J. D., 1996, Alluvial sediment, *in* Reading, H. G., Ed., Sedimentary environments: Processes, facies and stratigraphy, 3rd ed.: Blackwell Scientific Publications, Inc.

Deen, T. J., Gohl, K., Leslie, C., Papp, E., and Wake-Dyster, K., 2000, Seismic refraction inversion over a palaeochannel in the Lachlan fold belt, central NSW: Expl. Geophys., **31**, 389–393.

Downes, P. M., and Burton, G. R., 1999, Mineral occurrences in the Forbes district, *in* Forbes 1:250 000 geological sheet field conference guide: Aust. Geol. Sur. Organisation record 1999/20, 37–52.

Gibson, D. L., and Chan, R. A., 1999, Regolith and landscape mapping and evolution, *in* Forbes 1:250 000 geological sheet field conference guide: Aust. Geol. Sur. Organisation record 1999/20, 24–32.

Lanz, E., Maurer, H., and Green, A. G., 1998, Refraction tomography over a buried waste disposal site: Geophysics, **63**, 1414–1433.

Lawrie, K. C., 1999, Subsurface geophysical mapping of buried Tertiary palaeochannels for the 'Gilmore' project: AUSGEO News, April 1999.

Lawrie, K. C., Chan, R. A., Gibson, D. L., and de Souza Kovacs, N., 1999, Alluvial gold potential in buried palaeochannels in the Wyalong district, Lachlan fold belt, New South Wales: Aust. Geol. Sur. Organisation Res. Newsletter, **30**, 1–5.

Leslie, C., Jones, L., Papp, E., Wake-Dyster, K., Deen, T. J., and Gohl, K., 2000. High-resolution seismic imagery of palaeochannels near West Wyalong, NSW: Expl. Geophys., **31**, 383–388.

Mackey, T. E., Lawrie, K. C., Wilkes, P., Munday, T., de Souza Kovacs, N., Chan, R., Gibson, D., Chartres, C., and Evans, R., 2000, Palaeochannels near West Wyalong, New South Wales: A case study in delineation and modeling using aeromagnetics: Expl. Geophys., **31**, 1–7.

Munday, T. J., Reilly, N. S., Glover, M., Lawrie, K. C., Scott, T., Chartres, C. J., and Evans, W. R., 2000, Petrophysical characterisation of parna using ground and downhole geophysics at Marinna, central New South Wales: Expl. Geophys., **31**, 260–266.

Vidale, J. E., 1988, Finite-difference calculation of traveltimes: Bull. Seis. Soc. Am., **78**, 2062–2076.

——— 1990, Finite-difference calculation of traveltimes in three dimensions: Geophysics, **55**, 521–526.

Zelt, C. A., and Barton, P. J., 1998, Three-dimensional seismic refraction tomography: A comparison of two methods applied to data from the Faeroe basin: J. Geophys. Res., **103**, 7187–7210.